



**HAL**  
open science

## Control of Surface Segregation in Bimetallic NiCr Nanoalloys Immersed in Ag Matrix

Murtaza Bohra, Vidyadhar Singh, Panagiotis Grammatikopoulos, Evropi  
Toulkeridou, Rosa E. Diaz, Jean-François Bobo, Mukhles Sowwan

► **To cite this version:**

Murtaza Bohra, Vidyadhar Singh, Panagiotis Grammatikopoulos, Evropi Toulkeridou, Rosa E. Diaz, et al.. Control of Surface Segregation in Bimetallic NiCr Nanoalloys Immersed in Ag Matrix. Scientific Reports, 2016, 6 (1), 10.1038/srep19153 . hal-01718886

**HAL Id: hal-01718886**

**<https://hal.science/hal-01718886>**

Submitted on 18 Jun 2019

**HAL** is a multi-disciplinary open access archive for the deposit and dissemination of scientific research documents, whether they are published or not. The documents may come from teaching and research institutions in France or abroad, or from public or private research centers.

L'archive ouverte pluridisciplinaire **HAL**, est destinée au dépôt et à la diffusion de documents scientifiques de niveau recherche, publiés ou non, émanant des établissements d'enseignement et de recherche français ou étrangers, des laboratoires publics ou privés.

# SCIENTIFIC REPORTS

OPEN

## Control of Surface Segregation in Bimetallic NiCr Nanoalloys Immersed in Ag Matrix

Murtaza Bohra<sup>1,2</sup>, Vidyadhar Singh<sup>1</sup>, Panagiotis Grammatikopoulos<sup>1</sup>, Evropi Toulkeridou<sup>1</sup>, Rosa E. Diaz<sup>1</sup>, Jean-François Bobo<sup>3</sup> & Mukhles Sowwan<sup>1,4</sup>

Received: 19 October 2015  
Accepted: 07 December 2015  
Published: 11 January 2016

Cr-surface segregation is a main roadblock encumbering many magneto-biomedical applications of bimetallic M-Cr nanoalloys (where M = Fe, Co and Ni). To overcome this problem, we developed Ni<sub>95</sub>Cr<sub>5</sub>-Ag nanocomposite as a model system, consisting of non-interacting Ni<sub>95</sub>Cr<sub>5</sub> nanoalloys (5 ± 1 nm) immersed in non-magnetic Ag matrix by controlled simultaneous co-sputtering of Ni<sub>95</sub>Cr<sub>5</sub> and Ag. We employed Curie temperature ( $T_C$ ) as an indicator of phase purity check of these nanocomposites, which is estimated to be around the bulk Ni<sub>95</sub>Cr<sub>5</sub> value of 320 K. This confirms prevention of Cr-segregation and also entails effective control of surface oxidation. Compared to Cr-segregated Ni<sub>95</sub>Cr<sub>5</sub> nanoalloy films and nanoclusters, we did not observe any unwanted magnetic effects such as presence Cr-antiferromagnetic transition, large non-saturation, exchange bias behavior (if any) or uncompensated higher  $T_C$  values. These nanocomposites films also lose their unique magnetic properties only at elevated temperatures beyond application requirements ( $\geq 800$  K), either by showing Ni-type behavior or by a complete conversion into Ni/Cr-oxides in vacuum and air environment, respectively.

One of the foremost driving forces of current nano/biotechnology research is the ever-increasing need for new and smart magnetic nanomaterials that can be employed in a variety of applications encompassing magnetic resonance imaging (MRI), targeted drug delivery, giant magneto-resistive (GMR) sensors, induction-heating self-temperature controlling systems, etc.<sup>1–3</sup>. Often, a first line of attack in designing nanomaterials with tailored properties is to screen bulk material attributes for inspiration. Thus, the Ni<sub>95</sub>Cr<sub>5</sub> alloys<sup>1</sup>, showing a low Curie temperature ( $T_C \sim 320$  K), are certainly a very attractive candidate for several of the aforementioned applications.

Once a promising alloy has been selected, a nanostructure has to be designed and fabricated that maintains the desirable physical and chemical properties of the bulk reference system. However, synthesis of the Ni<sub>95</sub>Cr<sub>5</sub> nanoalloy with the desired  $T_C$  is rather challenging to start with, owing to a strong tendency for elemental demixing. Various types of inhomogeneous structures thus emerge, exhibiting  $T_C$  higher than the bulk value, and, in some cases, even attaining a pure-Ni bulk  $T_C$  value ( $\sim 625$  K), depending upon growth conditions<sup>4,5</sup>. For example, a recent study by the authors demonstrated the detrimental effect of element-specific Cr-surface segregation in vacuum; both NiCr alloy nanoparticles and NiCr thin films grown by gas-phase synthesis methods yielded high Ni-rich segregates of prohibitively high  $T_C$  values ( $> 470 - 500$  K)<sup>6</sup>. The origin of Cr-segregation was theoretically explained mainly on the basis of favorable energetics, since it resulted in overall potential energy minimization<sup>6</sup>. Ban *et al.* recently reported on successfully synthesizing by mechanical milling NiCr nanoalloys that show a low  $T_C \sim 325$  K, even though the increased Cr concentration they reported (Ni<sub>75</sub>Cr<sub>25</sub>) corresponds to a bulk alloy that displays non-magnetic behavior ( $\geq 13$  at.% Cr)<sup>4</sup>. They attributed this unexpected behavior to extensive heterogeneity in particle size distribution and composition, which is inherent to the fabrication method. Unfortunately, though, the  $T_C$  of their nanoparticles increased significantly when the samples were applied in a hyperthermia experiment, exactly due to this extensive heterogeneity.

<sup>1</sup>Nanoparticles by Design Unit, Okinawa Institute of Science and Technology Graduate University, 1919-1 Tancha Onna-Son, Okinawa, 904-0495, Japan. <sup>2</sup>Mahindra Ecole Centrale, Survey no: 62/1A, Bahadurpally Jeedimetla, Hyderabad-500043, Telangana India. <sup>3</sup>Centre d'Elaboration de Matériaux et d'Etudes Structurales (CEMES), 29 rue Jeanne Marvig, 31055 Toulouse Cedex 4, France. <sup>4</sup>Nanotechnology Research Laboratory, Al-Quds University, East Jerusalem, P.O. Box 51000, Palestine. Correspondence and requests for materials should be addressed to M.B. (email: murtaza@gmail.com) or M.S. (email: mukhles@oist.jp)

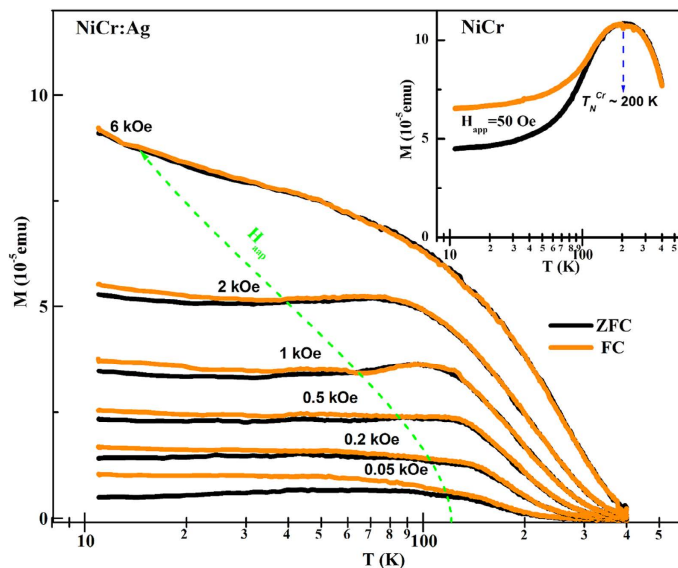


**Figure 1.** ZFC and FC magnetization curves of  $\text{Ni}_{95}\text{Cr}_5:\text{Ag}$  nanocomposite as a function of temperature (log scale). Measuring applied field  $H_{app}$ : 0.05 kOe; 0.2 kOe; 0.5 kOe; 1 kOe; 2 kOe; 6 kOe. Inset shows ZFC and FC magnetization curves measured at  $H_{app} = 0.05$  kOe for bare  $\text{Ni}_{95}\text{Cr}_5$  nanoalloy film.

Consequently, stability under working conditions is the ultimate criterion NiCr nanoalloys have to fulfill; otherwise, the end-product is merely an academic exercise. The nanostructure has to be tested with respect to its stability under realistic operational conditions, to assess its applicability range and determine its limitations. For example, air exposure is a common source of degradation for the magnetic properties of nanoalloys, as it induces selective oxidation and facilitates further segregation. When NiCr nanoalloys are exposed to air at ambient temperature, oxidation behavior is complicated and influenced by both Ni and Cr oxidation energies and rates of diffusion; in particular, by high preferential oxidation of Cr ions due to the high mobility of Cr in the host Ni matrix<sup>5,7</sup>. When the concentration of Cr is high, a  $\text{Cr}_2\text{O}_3$  surface layer forms, that potentially have some merits (e.g. for high corrosion-resistance applications)<sup>3,8</sup>. At 5% Cr, however, the full protective oxide layer cannot form; multi-site nucleation and coalescence of oxide particles ensues, leading to a core-satellite structure with possible cavity formation within the nanoparticle due to Kirkendall effect<sup>7</sup>, and ultimately resulting in deterioration of magnetic properties<sup>9</sup>. Annealing can also act as an additional degradation agent, enhancing demixing and converting  $\text{Ni}_{95}\text{Cr}_5$  nanoalloys into core-shell or -satellite type structures, instead of restoring the expected bulk magnetic structure<sup>6</sup>.

Therefore, precise control of elemental segregation is the key to maintain a desirable magnetic behavior. Various methods have been proposed to protect the magnetic nanoparticles/nanoalloys from surface oxidation<sup>10–14</sup>. Capping layers of metals are, generally, assumed to be a good barrier against oxidation, but recent findings by the authors<sup>11</sup> and work by Koch *et al.*<sup>12</sup> showed that post-deposition capping by noble metal Ag (~80 nm) is insufficient to shield Co nanoparticles (~7–14 nm in diameter) from surface oxidation, with the resultant effects in their magnetic properties. In contrast, De Toro *et al.*<sup>15</sup> demonstrated that diluted (<10 at.%) cluster-assembled granular Co:Cu films, prepared by simultaneous co-deposition of Co clusters with a Cu vapor, are perfectly stable under ambient conditions. Inspired by this work, and taking into account biocompatibility requirements for  $\text{Ni}_{95}\text{Cr}_5$  applications, herein we report on the development via simultaneous co-sputtering of  $\text{Ni}_{95}\text{Cr}_5:\text{Ag}$  nanocomposites with bulk Curie temperature values ( $T_C = 320$  K) and full control of Cr-segregation under working conditions.

## Results

In the present study, we synthesized  $\text{Ni}_{95}\text{Cr}_5:\text{Ag}$  nanocomposites using a co-sputtering process. As estimated by energy dispersive x-ray spectroscopy obtained with the Titan transmission electron microscope (TEM), they exhibit relative atomic concentrations around  $\text{Ni}_{95}\text{Cr}_5$  (~35%): Ag (~65%) (shown in supplementary Fig. S1a). Due to the abundance of Ag in our sample, as depicted in the high-resolution TEM (HRTEM) image (Fig. S1b), direct observation of the NiCr clusters alone is difficult. However, the strong correlation between structural and magnetic properties enables one to gather valuable information about the presence and structure of  $\text{Ni}_{95}\text{Cr}_5$  nanoalloy clusters embedded into the Ag matrix by conducting magnetic measurements.

To this end, the temperature dependence of magnetizations of these  $\text{Ni}_{95}\text{Cr}_5:\text{Ag}$  nanocomposites in ZFC (zero-field-cooled) and FC (field-cooled) conditions were recorded at various applied magnetic fields,  $H_{app}$ , from 0.05 to 6 kOe, as shown in Fig. 1. Various features of interest are present in this figure: first, the ZFC and FC curves almost coincide at high temperatures, but diverge markedly with decreasing temperatures. This constitutes first clear evidence for the presence of magnetic  $\text{Ni}_{95}\text{Cr}_5$  nanograins immersed in the non-magnetic Ag matrix. Moreover, a broad peak can be seen ending around the temperature range of 100–150 K in ZFC curve at low fields ( $H_{app} = 0.05$  kOe), which resembles the spin blocking temperature,  $T_B$ , above which  $\text{Ni}_{95}\text{Cr}_5$  nanograins should

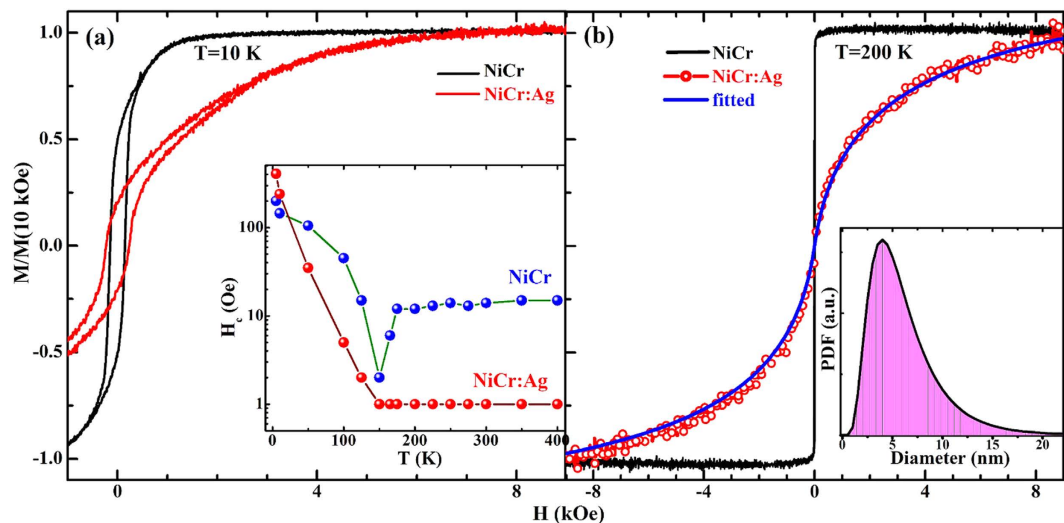


**Figure 2. Magnetic hysteresis behavior below and above blocking temperature of  $\text{Ni}_{95}\text{Cr}_5\text{:Ag}$  nanocomposite.** Normalized  $M-H$  loops for  $\text{Ni}_{95}\text{Cr}_5\text{:Ag}$  nanocomposite and  $\text{Ni}_{95}\text{Cr}_5$  nanoalloy films were taken at (a) 10 K and (b) 200 K. The inset of Fig. 2(a) shows  $H_c$  vs.  $T$  curves for both  $\text{Ni}_{95}\text{Cr}_5\text{:Ag}$  and  $\text{Ni}_{95}\text{Cr}_5$  films. The diameter distribution (probability density function) (inset of Fig. 2(b)) extracted from a Langevin fit [Eq. (1)] to 200 K  $M-H$  loops (blue color) of  $\text{Ni}_{95}\text{Cr}_5\text{:Ag}$ .

show superparamagnetic (SPM) behavior. The broad nature of the  $T_B$  peak emanates from the non-negligible size distribution of the  $\text{Ni}_{95}\text{Cr}_5$  nanograins. As  $H_{app}$  increases, the  $T_B$  peak moves towards low temperatures (as indicated by the green dotted line), eventually vanishing at  $H_{app}$  of 6 kOe, where ZFC and FC curves almost coincide with each other. Finally, as shown in Inset Fig. 1, bare  $\text{Ni}_{95}\text{Cr}_5$  films, without the presence of Ag, show an antiferromagnetic transition at temperature,  $T_N$ , around 200 K. This is a typical feature of Cr-segregation<sup>3</sup>, below which both FC and ZFC magnetizations decrease. Interestingly, the FC curve of the  $\text{Ni}_{95}\text{Cr}_5\text{:Ag}$  nanocomposite shows almost the temperature independent behavior below  $T_B$ ; thus, Cr-segregation was effectively prevented due to protection by the Ag matrix. The field-dependent ZFC peak ( $T_B$ ) and near-constant FC magnetization curves below  $T_B$  indicate spin-glass type features<sup>16–18</sup>, possibly due to a slight surface-spin disorder caused by interfacial interaction with the Ag matrix. Thus,  $\text{Ni}_{95}\text{Cr}_5$  nanograins behave more like a core-shell spin-structure with an ordered, ferromagnetic  $\text{Ni}_{95}\text{Cr}_5$  core, represented by  $T_B$ , surrounded by a spin-disordered shell.

For a better understanding of the observed SPM behavior, magnetization hysteresis (i.e.  $M-H$  loops) was measured as a function of applied magnetic field up to 10 kOe under ZFC conditions. Such representative normalized  $M-H$  loops, taken at 10 K for both  $\text{Ni}_{95}\text{Cr}_5\text{:Ag}$  and  $\text{Ni}_{95}\text{Cr}_5$  films, are shown in Fig. 2(a). The  $M-H$  loop of the  $\text{Ni}_{95}\text{Cr}_5\text{:Ag}$  nanocomposite (red curve) does not saturate easily under applied field of up to 8 kOe, compared to the low field ( $\leq 2$  kOe) required for the magnetically soft  $\text{Ni}_{95}\text{Cr}_5$  nanoalloy film (black curve). The coercivity value ( $H_c$ ) of the  $\text{Ni}_{95}\text{Cr}_5\text{:Ag}$  nanocomposite ( $\sim 265$  Oe) is almost twice as large as that of the  $\text{Ni}_{95}\text{Cr}_5$  nanoalloy ( $\sim 135$  Oe). There could be many possible reasons for this observation, such as enhancement in surface anisotropy due to the interfacial roughness of Ag/ $\text{Ni}_{95}\text{Cr}_5$  (discussed in below) causing a more canted-type  $\text{Ni}_{95}\text{Cr}_5$  core spin structure; alternatively, interface contact of the  $\text{Ni}_{95}\text{Cr}_5$ -nanoalloy with the Ag matrix can result in some hybridization of Ag and  $\text{Ni}_{95}\text{Cr}_5$  orbitals, as has been explained elsewhere<sup>10–11</sup>. Strikingly,  $H_c$  values of the  $\text{Ni}_{95}\text{Cr}_5\text{:Ag}$  nanocomposite, deduced from  $M-H$  loops measured between 5–400 K, almost fall to zero above the blocking temperature,  $T_B = 150$  K, clearly indicating SPM  $\text{Ni}_{95}\text{Cr}_5$  nanograins in the Ag matrix (Inset of Fig. 2(a)). Around the same temperature ( $T_B$ ), the magnetoresistance value (shown in supplementary information Fig. S2) of  $\text{Ni}_{95}\text{Cr}_5\text{:Ag}$  nanocomposite abruptly decreases from 0.9% to 0%, clearly verifying the SPM behavior of  $\text{Ni}_{95}\text{Cr}_5$  nanograins in Ag matrix.

Another meaningful conclusion can be drawn from the temperature dependence of  $H_c$  values of the  $\text{Ni}_{95}\text{Cr}_5$  nanoalloy film (Inset of Fig. 2(a)) which show sharp minima around the antiferromagnetic transition temperature ( $T_N$ ) 150 K of Cr. The low value of  $T_N$  compared to the bulk Cr value (315 K)<sup>5,7,9</sup>, can be attributed to the nano sizes of Cr-segregates. These samples also display step-type  $M-H$  loops with a constant  $H_c$  value (15 Oe) above  $T_N$ , which is an expected feature of NiCr nanoalloys, but the increase of the  $H_c$  value below  $T_N$  can be attributed to the uncompensated magnetization of NiCr cores over Cr-segregates. We did not observe such features in  $\text{Ni}_{95}\text{Cr}_5\text{:Ag}$  nanocomposite (brown curve), which, once more, supports our argument that the  $\text{Ni}_{95}\text{Cr}_5\text{:Ag}$  nanocomposite does not show any Cr-segregation. In the present case, the  $T_N$  of the  $\text{Ni}_{95}\text{Cr}_5$  nanoalloy films (150 K) and the  $T_B$  of the  $\text{Ni}_{95}\text{Cr}_5\text{:Ag}$  nanocomposite (120 K) are found to be close, but one should not confuse them, since the  $\text{Ni}_{95}\text{Cr}_5\text{:Ag}$  nanocomposite shows zero  $H_c$  values above  $T_B$  due to SPM behavior, as opposed to the non-zero constant value in case of the  $\text{Ni}_{95}\text{Cr}_5$  nanoalloy film.

The exact size range of the core NiCr nanograins was investigated next. SPM  $\text{Ni}_{95}\text{Cr}_5$  nanograins show typical S-shape  $M-H$  loop above  $T_B$  (200 K, presented in Fig. 2(b)), with zero  $H_c$  and remnant magnetization values.

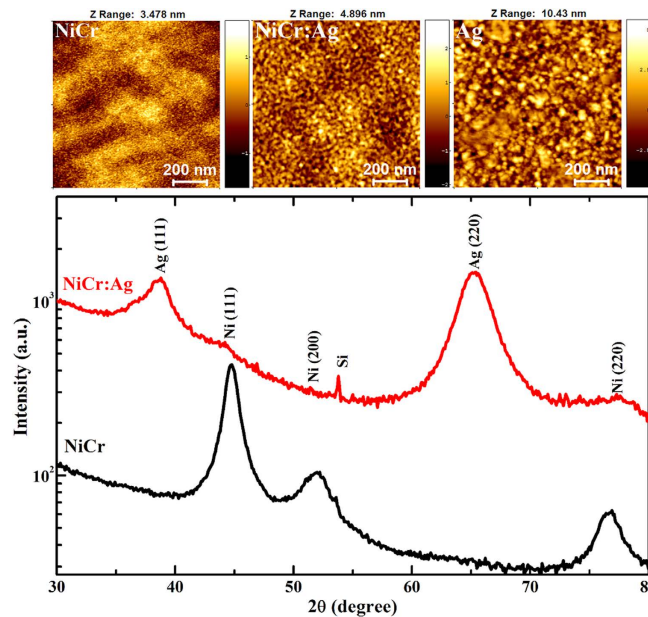


**Figure 3. Crystalline structure and surface morphology of  $\text{Ni}_{95}\text{Cr}_5\text{:Ag}$  nanocomposite and  $\text{Ni}_{95}\text{Cr}_5$  film.** GIXRD patterns of  $\text{Ni}_{95}\text{Cr}_5\text{:Ag}$  nanocomposite and  $\text{Ni}_{95}\text{Cr}_5$  nanoalloy film. AFM images of  $\text{Ni}_{95}\text{Cr}_5$ ,  $\text{Ni}_{95}\text{Cr}_5\text{:Ag}$  and Ag films (over  $1\ \mu\text{m} \times 1\ \mu\text{m}$  area) are shown in upper panel. The measured RMS roughness values are 0.380, 0.532, and 1.319 nm for the as deposited  $\text{Ni}_{95}\text{Cr}_5$ ,  $\text{Ni}_{95}\text{Cr}_5\text{:Ag}$  and Ag film, respectively.

The  $M-H$  loops of ideal SPM non-interacting nanoparticles of various sizes can be fitted by a log-normal moment-weighted Langevin function<sup>19</sup>:

$$M(H) = N \int_0^\infty \mu L\left(\frac{\mu H}{k_B T}\right) f(\mu) d\mu \quad (1)$$

where  $L(x) = \coth(x) - 1/x$ ,  $x = \mu H/k_B T$  is the Langevin function and

$$f(\mu) = \frac{1}{\sigma \mu_0 \sqrt{2\pi}} e^{-\left[\frac{\ln\left(\frac{\mu}{\mu_0}\right)^2}{2\sigma^2}\right]} \quad (2)$$

is the log-normal distribution, where  $\mu_0$  is the median moment and  $\sigma$  is the standard deviation of  $\ln(\mu/\mu_0)$ , respectively. These distribution parameters,  $\mu_0$  and  $\sigma$ , are estimated by fitting Eq. (1) to the  $M-H$  data of 200 K (*i.e.* above  $T_B$ ). From our best fit shown in Fig. 2(b) (blue line), we deduced a log-normal distribution (Inset of Fig. 2(b)) of core diameters with mean diameter value  $D_0 = 5.32 \pm 0.542$  nm.

Because of the small sizes of  $\text{Ni}_{95}\text{Cr}_5$  grains in the Ag matrix, the GIXRD (lower panel of Fig. 3) pattern shows only faint ‘shoulders’ around the position of FCC-Ni (111) and (220) peaks compared to the  $\text{Ni}_{95}\text{Cr}_5$  nanoalloy. The corresponding surface morphology changes can be seen in AFM images (upper panel of Fig. 3), with a sharp reduction in surface RMS roughness in  $\text{Ni}_{95}\text{Cr}_5\text{:Ag}$  nanocomposite film ( $\sim 0.532$  nm) compared to pure Ag film ( $\sim 1.319$  nm). Surface roughness is highly dependent on deposition rate, grain size and thickness of films<sup>11</sup>. The  $\text{Ni}_{95}\text{Cr}_5$  film shows reduced roughness due to lower deposition rate and smaller grain size compared to the Ag film. The roughness changes in the  $\text{Ni}_{95}\text{Cr}_5\text{:Ag}$  case, where there are altogether different grain sizes. The GIXRD pattern does not show any impurity antiferromagnetic phases such as Cr,  $\text{CrO}_2$ ,  $\text{Cr}_2\text{O}_3$  or NiO, which is further confirmed by exchange bias study (shown in supplementary information Fig. S3) at 3 K, a method described elsewhere<sup>11,20</sup>.

Prevention of Cr-segregation is, of course, just a means to an end; the main goal is to preserve the desired magnetic properties of bulk NiCr in the nanoscale, for targeted applications. To investigate whether this goal was achieved, normalized FC magnetization  $M(T)/M(10\ \text{K})$  measured under an applied field of  $H_{app} = 1$  kOe in the temperature range  $5\ \text{K} \leq T \leq 400\ \text{K}$  for  $\text{Ni}_{95}\text{Cr}_5\text{:Ag}$  nanocomposite and  $\text{Ni}_{95}\text{Cr}_5$  nanoalloy are shown in Fig. 4. The  $M-T$  data of bulk  $\text{Ni}_{95}\text{Cr}_5$  alloy is also given in the same figure for comparison. The ratio  $M/H$  closely approximates the initial differential susceptibility  $\chi = dM/dH$  so that a rough  $T_C$  estimation can be achieved without substantial field-induced broadening. The  $M(T)/M(10\ \text{K})$  vs. temperature curve of  $\text{Ni}_{95}\text{Cr}_5\text{:Ag}$  nanocomposite shows qualitatively different behavior from that of the ordered bulk  $\text{Ni}_{95}\text{Cr}_5$  alloy, with its magnetization decreasing earlier, in the temperature range 100–400 K; however, it displays the same  $T_C$  as the bulk sample.

Let us scrutinize this observation a bit further. Amekura *et al.*<sup>21</sup> observed similar behavior in SPM Ni nanoparticles ( $\sim 3$  nm) embedded in  $\text{SiO}_2$  matrix; however, a small but non-zero value of magnetization remained in the

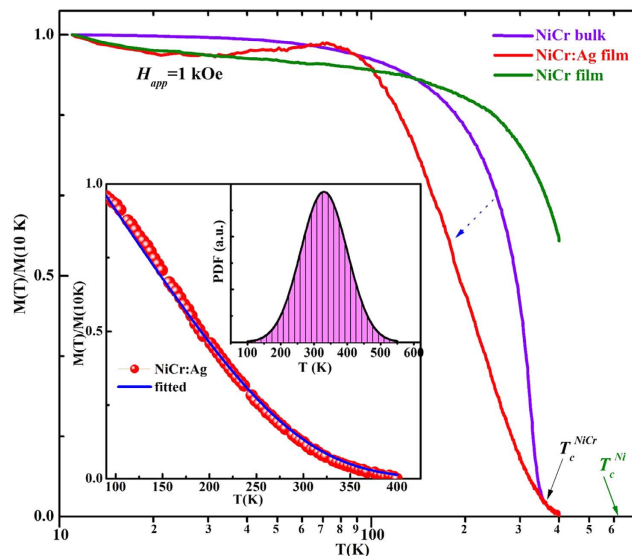


**Figure 4. Curie temperature ( $T_C$ ) determination of  $\text{Ni}_{95}\text{Cr}_5\text{:Ag}$  nanocomposite and  $\text{Ni}_{95}\text{Cr}_5$  film.** Normalized magnetizations at fixed field,  $H_{app} = 1$  kOe, as a function of temperature,  $T$ , (log scale) for  $\text{Ni}_{95}\text{Cr}_5\text{:Ag}$  nanocomposite, and  $\text{Ni}_{95}\text{Cr}_5$  nanoalloy films along with bulk  $\text{Ni}_{95}\text{Cr}_5$  alloy. The inset shows the fitted data to Eq. (4) of  $\text{Ni}_{95}\text{Cr}_5\text{:Ag}$  nanocomposite in the critical range 90–400 K, which results in  $T_C$  distribution (probability density function).

nanoparticles even above the bulk  $T_C$ . They ascribed this to the finite size effects of nanoparticles using quantum Monte-Carlo simulation. Skomski *et al.*<sup>22</sup> also predicted similar results for the  $T_C$  of interaction-free multiphase nanostructures theoretically, and argued that in nanocomposites there can only be one  $T_C$  regardless of the bulk Curie temperatures of the phases involved. The  $T_C$  is higher than the volume average of the Curie temperatures of the individual phases. Skomski *et al.*<sup>22</sup> also explained that because of the non-relativistic character of the interatomic exchange, the  $T_C$  coupling range is atomic rather than nanoscale, so that the comparatively high Curie temperatures of nanocomposites do not translate into an enhanced permanent-magnet energy product ( $B-H$ ), i.e. hysteresis. In a similar fashion, our  $\text{Ni}_{95}\text{Cr}_5\text{:Ag}$  nanocomposite contains a great (approximately infinite) number of SPM clusters, which do not interact with each other above  $T_B$ , due to the presence of the Ag matrix. Each cluster is characterized by a specific  $T_C$  value, and its magnetization near this  $T_C$  follows the general power law<sup>23</sup> given by:

$$M(T, T_C) = M_0 \left( \frac{T_C - T}{T_C} \right)^\beta \theta(T_C - T) \quad (3)$$

where  $M_0$  is a factor proportional to the saturation magnetization, and  $\theta$  is the Heaviside function, pinning  $M$  to zero for temperatures above  $T_C$ , thus warranting that the material has entered its paramagnetic phase<sup>23</sup>. The overall magnetization of the model thin film can be derived by<sup>23</sup>:

$$M(T) = \int_0^{+\infty} M_0 \left( \frac{T_C - T}{T_C} \right)^\beta \theta(T_C - T) \frac{1}{\sigma\sqrt{2\pi}} e^{-\frac{(T_C - \mu)^2}{2\sigma^2}} dT_C \quad (4)$$

where  $\sigma$  and  $\mu$  is the  $T_C$  variance and mean of distribution, respectively. We fitted the parameters of this function to the experimental magnetization graph at elevated temperatures, near  $T_C$  using the least squares method, assuming that the mean of distribution ( $\mu$ ) is the  $T_C$  obtained experimentally (330 K). Our best fit is shown in Inset of Fig. 4, along with the probability distribution function (PDF) plot, for  $\sigma = 70$  K and  $\beta = 1.12$ , showing excellent agreement with the experiment. Some part of the  $T_C$  distribution (around  $\sim 5-12$  K) can be attributed to applied field induced broadening,<sup>23</sup> however, the remaining  $T_C$  distribution is ascribed to the intrinsic contribution of different sizes of  $\text{Ni}_{95}\text{Cr}_5$  nanograins in the Ag matrix. Thus, our  $\text{Ni}_{95}\text{Cr}_5\text{:Ag}$  nanocomposite indeed exhibit a  $T_C$  distribution around the bulk  $\text{Ni}_{95}\text{Cr}_5$  alloy  $T_C$  value under control conditions.

To demonstrate the effectiveness of our method in protecting Cr-segregation, it is imperative to emphasize that the magnetization of the bare  $\text{Ni}_{95}\text{Cr}_5$  nanoalloy (green curve, Fig. 4) does not vanish at bulk  $\text{Ni}_{95}\text{Cr}_5$   $T_C$  value of around 320 K, clearly suffering from Cr-segregation, with the resultant deterioration of its magnetic behavior. Even though the thermal demagnetization process of our  $\text{Ni}_{95}\text{Cr}_5\text{:Ag}$  nanocomposite is somewhat different than of the bulk  $\text{Ni}_{95}\text{Cr}_5$ , the complete loss of magnetization happens at around the same temperature as with bulk  $\text{Ni}_{95}\text{Cr}_5$  alloy, which rules out any possibility of Cr-segregation in our  $\text{Ni}_{95}\text{Cr}_5\text{:Ag}$  nanocomposite.

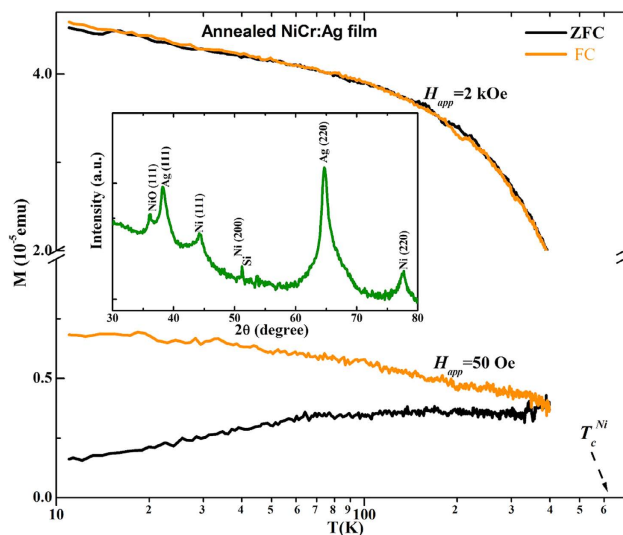


**Figure 5. Structural and magnetic property change after post annealing.** ZFC and FC magnetizations as function of temperature,  $T$ , (log scale) measured at a fixed field of 50 Oe and 2 kOe for annealed  $\text{Ni}_{95}\text{Cr}_5\text{:Ag}$  nanocomposite. The inset shows GIXRD pattern of annealed  $\text{Ni}_{95}\text{Cr}_5\text{:Ag}$  nanocomposite.

## Discussion

After protecting  $\text{Ni}_{95}\text{Cr}_5$  nanoalloys in Ag matrix from suffering Cr-surface segregation, it is informative to test the temperature limitations of our methods by comparing the magnetic properties of the  $\text{Ni}_{95}\text{Cr}_5\text{:Ag}$  nanocomposite before and after annealing. The temperature dependence of ZFC and FC magnetizations curve measured at low (50 Oe) and high field (2 kOe) for  $\text{Ni}_{95}\text{Cr}_5\text{:Ag}$  nanocomposites annealed at 450 °C under vacuum of  $1 \times 10^{-7}$  mbar are plotted in Fig. 5. A large difference between ZFC and FC magnetizations (at 50 Oe) starting well above room temperature can be observed, indicating a higher  $T_B \geq 400$  K, whereas for the same field as-deposited  $\text{Ni}_{95}\text{Cr}_5\text{:Ag}$  nanocomposite show low  $T_B$  around 100 K. This difference clearly indicates an enlargement of effective magnetic volume due to either increased  $\text{Ni}_{95}\text{Cr}_5$  particle sizes or Cr-segregation in the Ag non-magnetic matrix upon annealing.

This is further supported by the GIXRD result of the Inset of Fig. 5, showing much sharper Ni peaks compared to those of the as-deposited film (Fig. 3, red curve). FCC Ni (111), (200) and (220) diffraction peaks obviously appear, signifying the formation and precipitation of FCC  $\text{Ni}_{95}\text{Cr}_5$ -rich particles of sizes  $\sim 10$ – $12$  nm (estimated by the Scherrer formula<sup>24</sup>) from the Ag-matrix. It is worth mentioning here that the addition of such a small percentage of Cr does not offset the XRD peak positions of Ni noticeably, because it hardly induces any significant change in the Ni lattice<sup>25</sup>. The NiO (111) peak can only be observed due to surface oxidation of  $\text{Ni}_{95}\text{Cr}_5$  nanoparticles of a relatively larger size, as they emerge from the Ag matrix after annealing and get exposed to air during transfer for the GIXRD measurement. These results are in agreement with observations reported on Ni-Ag, Co:Ag and Co:Cu nanogranular systems<sup>25–28</sup>. In the GIXRD of the as-deposited  $\text{Ni}_{95}\text{Cr}_5\text{:Ag}$  nanocomposite,  $\text{Ni}_{95}\text{Cr}_5$ -rich particles cannot be seen clearly, due to the formation of very small clusters and the metastable alloying with Ag. Although it is known that at equilibrium conditions the mutual solubility of  $\text{Ni}_{95}\text{Cr}_5$  and Ag is very low, the use of a non-equilibrium deposition process such as sputtering at room temperature allowed a substantial concentration of  $\text{Ni}_{95}\text{Cr}_5$  clusters to dissolve, forming  $\text{Ni}_{95}\text{Cr}_5\text{:Ag}$  nanocomposites;<sup>26–29</sup> their concentration, however, was reduced after annealing, through an extensive demixing process.

At high field (2 kOe), ZFC and FC magnetizations overlap and do not vanish at bulk  $\text{Ni}_{95}\text{Cr}_5$  alloy  $T_C$  value of 320 K, but instead approach towards Ni bulk  $T_C$  values similar to the  $\text{Ni}_{95}\text{Cr}_5$  nanoalloy films (Fig. 4, green curve), showing that some Cr-segregation is also caused by annealing. Similar behavior was observed previously in pure  $\text{Ni}_{95}\text{Cr}_5$  nanoclusters after annealing<sup>6</sup>. Therefore, there are two simultaneous segregation mechanisms at play:  $\text{Ni}_{95}\text{Cr}_5$  nanograins segregating from the Ag matrix, due to dewetting, and precipitating into larger  $\text{Ni}_{95}\text{Cr}_5$  grains also allow for Cr-surface segregation in each one of these grains. Their combination eventually enhances Ni–Ni particle interactions,<sup>6,9</sup> as a result, bulk-Ni magnetic properties (higher  $T_B$  and  $T_C$  values) are expected. It should be stressed, however, that annealing took place at distinctly higher temperatures than those required for potential applications of our nanocomposite, and, unlike previously reported case-studies, imposes no practical limitation in the utilization of our method.

In summary, this study tackles a frequent problem of bimetallic M-Cr nanoalloys: that of Cr-surface segregation, with the resultant deterioration of magnetic properties.  $\text{Ni}_{95}\text{Cr}_5$  nanoalloys were synthesized, immersed in a non-magnetic Ag matrix via a direct co-sputtering technique. The strong correlation between structure and magnetic properties enabled the collection of information about the structure of the nanoalloys by performing magnetic measurements. Low-temperature divergence of ZFC and FC magnetizations certified the presence of  $\text{Ni}_{95}\text{Cr}_5$  nanoalloys of a non-negligible size distribution. The observed SPM behavior of the nanocomposite was investigated by measuring magnetization hysteresis; indeed, the  $H_c$  value dropping to zero above the  $T_B$  not only re-confirmed the presence of SPM  $\text{Ni}_{95}\text{Cr}_5$  nanoalloys in the Ag matrix, but also revealed their size distribution.

Most importantly, averting Cr from demixing preserves the desired magnetic properties of bulk NiCr (e.g.  $T_C$ ) in the nanoscale for targeted applications, such as magnetic hyperthermia for cancer treatment. Once more, the necessity for the segregation prevention method was confirmed by demonstrating that without the presence of the Ag matrix Ni<sub>95</sub>Cr<sub>5</sub> nanoalloys unequivocally suffer from Cr-segregation. Finally, temperature limitations for the usage of our method were tested by comparing magnetic properties of the Ni<sub>95</sub>Cr<sub>5</sub>:Ag nanocomposite before and after annealing.

## Methods

**Nanocomposite growth.** The Ni<sub>95</sub>Cr<sub>5</sub>:Ag nanocomposite films (~80 nm thick) were fabricated by a co-sputtering technique, and deposited on Si and fused quartz substrates at ambient temperature. Schematic diagram of experimental setup is shown in Fig. S4. The composition was adjusted by optimizing the DC magnetron sputtering power of the Ni<sub>95</sub>Cr<sub>5</sub> (40 W) and Ag (20 W) targets while maintaining Ar pressure at  $2.7 \times 10^{-3}$  mbar. The deposit thickness rate was measured by using a quartz-crystal monitor. We deliberately chose a deposition rate with a low Ni<sub>95</sub>Cr<sub>5</sub> (0.04 nm/s) volume fraction, so that the Ni<sub>95</sub>Cr<sub>5</sub> particles remained isolated in the Ag medium. To ensure that they were fully capped by a layer of Ag, we prolonged the deposition of Ag (0.09 nm/s). Substrate table rotation was set at 2 rpm for all depositions, to ensure uniform film deposition. To investigate the effect of post-thermal treatment, the nanocomposites were subsequently annealed under vacuum lower than  $1 \times 10^{-7}$  mbar for 60 minute at 450 °C in the deposition chamber. Nanoalloy Ni<sub>95</sub>Cr<sub>5</sub> thin films were also deposited under the same sputtering power (40 W) for comparative study.

**Surface morphology and Compositional analysis.** After substrate landing, nanocomposite-loaded Si (100) substrates were load-lock transferred to an inert gas (N<sub>2</sub>) glove-box and surface morphology was characterized by atomic force microscopy (AFM) using a Multimode 8 (Bruker, Santa Barbara, CA) instrument operating in tapping mode. The AFM system height “Z” resolution and noise floor are less than 0.030 nm. The scanning probe processor (SPIP) (Image Metrology, Hørsholm, DK) software was employed for the root-mean-square (RMS) roughness analysis. Nanocomposite structures were characterized using both grazing incidence x-ray diffraction (GIXRD, Bruker D8 Discover XRD<sup>2</sup> system with Cu K<sub>α</sub> x-ray source) at grazing angle of 0.25° and Cs-corrected transmission electron microscopy (TEM, FEI Titan G2<sup>TM</sup> 80–300 kV) operating at 300 kV. The annular bright-field (ABF) image was taken on a scanning transmission electron microscope. Energy dispersive x-ray spectroscopy was performed with an Oxford Xmax system, with an 80 mm<sup>2</sup> silicon drift detector (SDD) and energy resolution of 136 eV.

**Magnetic measurements.** The magnetic properties of the as-deposited and annealed films were measured with in-plane configuration in a Quantum Design physical property measurement system (PPMS<sup>TM</sup>) using vibrating sample magnetometer (VSM, 2–400 K). Magnetization as a function of applied magnetic field,  $M-H$ , loops were taken at various temperatures between 5 and 400 K. The diamagnetic contribution from the Si substrate, glue and Ag was subtracted from magnetization data by measuring the high-field magnetic susceptibility. For zero-field-cooled (ZFC) magnetization measurements, the sample was initially cooled to 5 K in zero field, and subsequently magnetizations were measured under various fixed fields upon heating. Next, the field-cooled (FC) magnetization was recorded during cooling for each field.

## References

- Akin, Y., Obaidat, I. M., Issa, B. & Haik, Y. Ni<sub>1-x</sub>Cr<sub>x</sub> alloy for self-controlled magnetic hyperthermia. *Cryst. Res. Technol.* **44**, 386 (2009).
- Thompson, J. R., Goyal, A., Christen, D. K. & Kroeger, D. M. Ni-Cr textured substrates with reduced ferromagnetism for coated conductor applications. *Physica C: Superconductivity* **370**, 169 (2002).
- Kaur, M. *et al.* Watermelon-like iron nanoparticles: Cr doping effect on magnetism and magnetization interaction reversal. *Nanoscale* **5**, 7872–7881 (2013).
- Ban, I., Stergar, J., Drogenik, M., Ferk, G. & Makovec, D. Synthesis of chromium-nickel nanoparticles prepared by a microemulsion method and mechanical milling. *Acta Chim. Slov.* **60**, 750 (2013).
- Wang, C. M. *et al.* Microstructure of the native oxide layer on Ni and Cr-doped Ni nanoparticles. *J Nanosci Nanotechnol.* **11**, 8488 (2011).
- Bohra, M. *et al.* Surface segregation in Cr-doped NiCr alloy nanoparticles and its effect on their magnetic behavior. *Chem. Mater.* **27**, 3216–3225 (2015).
- Wang, C. M. *et al.* In-situ TEM visualization of vacancy injection and chemical partition during oxidation of Ni-Cr nanoparticles. *Sci. Rep.* **4**, 3683 (2014).
- Gich, M. *et al.* Aerosol nanoparticles in the Fe<sub>1-x</sub>Cr<sub>x</sub> system: Room-temperature stabilization of the  $\sigma$  phase and  $\sigma \rightarrow \alpha$ -phase transformation. *J. Appl. Phys.* **98**, 024303 (2005).
- Sundararajan, J. A. *et al.* Heat treatment on Ni and Cr-doped Ni core-shell nanoparticle granular films. *Nanotechnology (IEEE-NANO): 2011 11<sup>th</sup> IEEE Conference on*, Portland, OR. IEEE. (doi:10.1109/NANO.2011.6144472) (2011, 15–18 Aug.).
- Ebbing, A., Hellwig, O., Agudo, L., Eggeler, G. & Petravic, O. Tuning the magnetic properties of Co nanoparticles by Pt capping. *Phys. Rev. B* **84**, 012405 (2011).
- Bohra, M. *et al.* Influence of packaging on the surface oxidation and magnetic properties of cobalt nanocrystals. *J. Phys. D: Appl. Phys.* **47**, 305002 (2014).
- Koch, S. A. *et al.* Magnetic and structural properties of Co nanocluster thin films. *Phys. Rev. B* **71**, 085410 (2005).
- Özkale, B. *et al.* One-pot electrosynthesis of multi-layered magnetic metallopolymer nanocomposites. *Nanoscale*, **6**, 4683–4690 (2014).
- Singh, V., Srinivas, V., Ranot, M., Angappane, S. & Park, J.-G. Effect of polymer coating on the magnetic properties of oxygen-stabilized nickel nanoparticles. *Phys. Rev. B* **82**, 054417 (2010).
- De Toro, J. A., Andrés, J. P., González, J. A., Muñoz, P. & Riveiro, J. M. The oxidation of metal-capped Co cluster films under ambient conditions. *Nanotechnology*, **20**, 085710 (2009).
- He, L. *et al.* Size-dependent magnetic properties of nickel nanochains. *J. Phys. Condens. Matter*, **19**, 036216 (2007).

17. Elovaara, T., Huhtinen, H., Majumdar, S. & Paturi, P. Linear and nonlinear ac susceptibilities in polycrystalline low-bandwidth  $\text{Pr}_{1-x}\text{Ca}_x\text{MnO}_3$  ( $x = 0.0-0.3$ ) manganite. *J. Phys.: Condens. Matter*, **26**, 266005 (2014).
18. Bandyopadhyay, M. & Dattagupta, S. Memory in nanomagnetic systems: Superparamagnetism versus spinglass behavior. *Phys. Rev. B* **74**, 214410 (2006).
19. De Toro, J. A. *et al.* Energy barrier enhancement by weak magnetic interactions in Co/Nb granular films assembled by inert gas condensation. *Phys. Rev. B* **85**, 054429 (2012).
20. López Antón, R. *et al.* High-vacuum annealing reduction of Co/CoO nanoparticles. *Nanotechnology*, **25**, 105702 (2014).
21. Amekura, H., Fudamoto, Y., Takeda, Y. & Kishimoto, N. Curie transition of superparamagnetic nickel nanoparticles in silica glass: A phase transition in a finite size system. *Phys. Rev. B* **71**, 172404 (2005).
22. Skomski, R. & Sellmyer, D. J. Curie temperature of multiphase nanostructures. *J. Appl. Phys.* **87**, 4756 (2000).
23. Campillo, G. *et al.* Substrate dependence of magnetic properties of  $\text{La}_{0.67}\text{Ca}_{0.33}\text{MnO}_3$  films. *J. Magn. Magn. Mater.* **237**, 61–68 (2001).
24. Alexander L. & Klug, H. P. Determination of crystallite size with the x-ray spectrometer. *J. Appl. Phys.* **21**, 137 (1950).
25. Wang, C. M. *et al.* Microstructure of the native oxide layer on Ni and Cr-doped Ni nanoparticles. *J Nanosci Nanotechnol.* **11**, 8488 (2011).
26. Santhi, K. *et al.* Synthesis, structure stability and magnetic properties of nanocrystalline Ag–Ni alloy. *J Nanopart Res* **14**, 868 (2012).
27. Du, J., Zhang, B., Zheng, R. K. & Zhang, X. X. Memory effect and spin-glass-like behavior in Co–Ag granular films. *Phys. Rev. B*, **75**, 014415 (2007).
28. John, Q., Xiao, J., Samuel, J. & Chien, C. L. Giant magnetoresistance in the granular Co–Ag system. *Phys. Rev. B*, **46**, 9266 (1992).
29. De Toro, J. A. *et al.* Improved giant magnetoresistance in nanogranular Co/Ag: The role of interparticle RKKY interactions, *Phys. Rev. B* **70**, 224412 (2004).

## Acknowledgements

This work was supported by funding from the Okinawa Institute of Science and Technology Graduate University.

## Author Contributions

M.B. performed the magnetic and GIXRD measurements. V.S. performed sample deposition and AFM measurements. R.E.D. performed the TEM imaging. M.B., V.S., P.G. and E.T. and J.F.B. analyzed the magnetic data. P.G. prepared the schematics sketch of Figure S4. M.S. conceived the idea and supervised the project. All authors contributed to writing and editing the manuscript.

## Additional Information

**Supplementary information** accompanies this paper at <http://www.nature.com/srep>

**Competing financial interests:** The authors declare no competing financial interests.

**How to cite this article:** Bohra, M. *et al.* Control of Surface Segregation in Bimetallic NiCr Nanoalloys Immersed in Ag Matrix. *Sci. Rep.* **6**, 19153; doi: 10.1038/srep19153 (2016).



This work is licensed under a Creative Commons Attribution 4.0 International License. The images or other third party material in this article are included in the article's Creative Commons license, unless indicated otherwise in the credit line; if the material is not included under the Creative Commons license, users will need to obtain permission from the license holder to reproduce the material. To view a copy of this license, visit <http://creativecommons.org/licenses/by/4.0/>